Nanopore Analysis of Single-Stranded Binding Protein Interactions with DNA
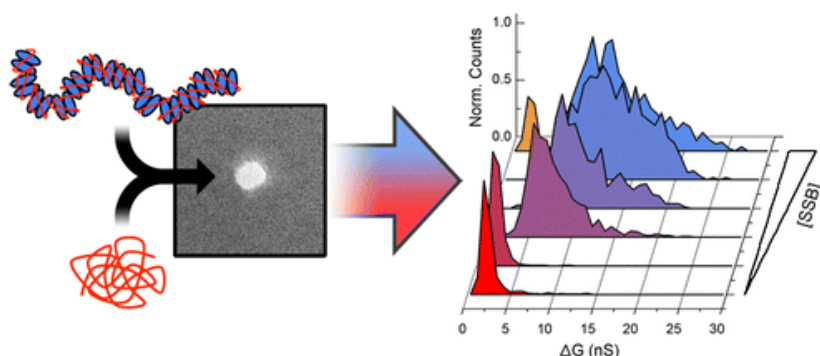
By: Michael M. Marshall, Jan Ruzicka, Osama K. Zahid, Vincent C. Henrich, Ethan W. Taylor, and Adam R. Hall

Abstract:

We study the binding of *E. coli* single-stranded binding protein (SSB) to single-stranded DNA (ssDNA) using a solid-state nanopore assay. We find that saturated nucleoprotein complexes can be distinguished easily from free SSB, ssDNA, or double-stranded DNA individually and demonstrate that the high affinity of SSB for ssDNA can be exploited to achieve high-fidelity differentiation from duplex molecules in a mixture. We then study nucleoprotein filament formation by systematically varying the amount of SSB relative to ssDNA. We observe a concomitant shift in the mean amplitude of electrical events that is consistent with weakly cooperative binding. Finally, we compare circular and linearized ssDNA saturated with SSB and use the results to infer structural details of the nucleoprotein complex.

Keywords: single-stranded binding protein | *E. coli* | single-stranded DNA | nucleoprotein complex

Article:

Introduction

Single-stranded binding proteins (SSB) occur ubiquitously in nature and are believed to be present in all organisms. SSBs are known to be important in DNA recombination, repair, and replication[1, 2] but have also been shown to play a central role in a wide variety of other processes, including telomere regulation[3] and tumor suppression[4] in humans, transcription in plants,[5] and protection from ionizing radiation in extremophiles.[6] Given this diverse biological significance, the development of new approaches for studying SSB interactions with DNA remains an important research goal.

A typical model SSB is that of *E. coli*, a stable homotetramer with a net molecular weight of 74 kDa. While there is no sequence specificity associated with the interaction of *E. coli* SSB with ssDNA, the number of nucleotides involved in its binding, n, can vary on the basis of experimental conditions such as ionic concentration. This site size $(SSB)_n$ is an important consideration that informs both structural and quantitative inferences.[2] Experimental evidence suggests that three different binding modes are possible with ssDNA: $(SSB)_{35}$ in which two SSB subunits are bound at low ionic strength; $(SSB)_{56}$ in which all four subunits have some interaction at intermediate ionic strength; and $(SSB)_{65}$ in which all four subunits are stably bound at high salt concentration.
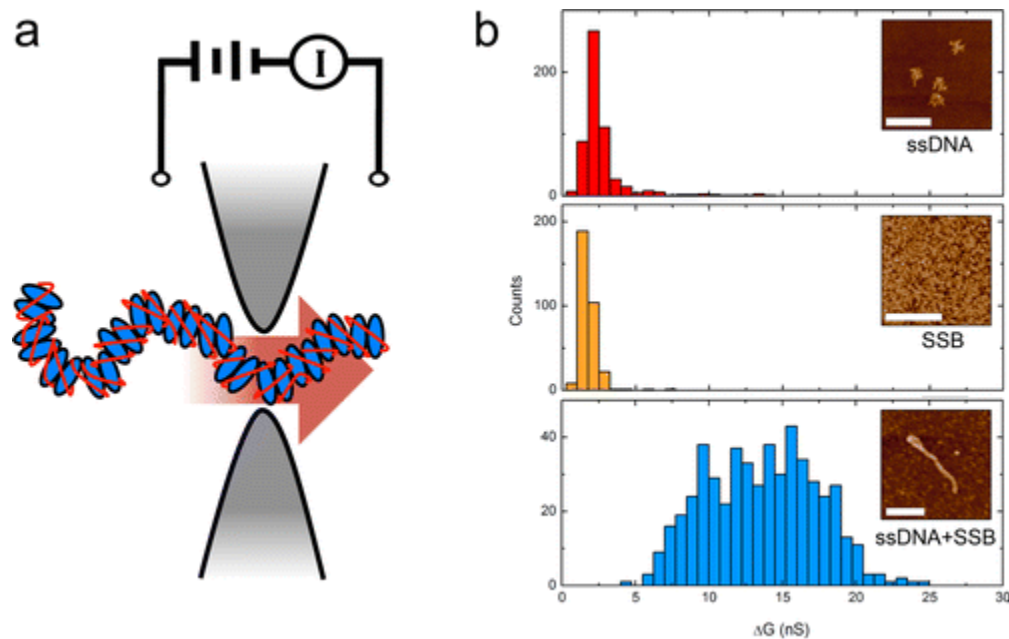

Figure 1. SS-nanopore detection of SSB-ssDNA. (a) Schematic picture of measurement depicting a SSB-ssDNA nucleoprotein filament being translocated through a SS-nanopore electrically. (b) Mean event amplitude histograms for translocations of ssDNA alone (red, $n = 551$), SSB alone (orange, $n = 327$), and an incubated mixture of ssDNA with SSB (1:284; blue, $n = 824$). Insets show atomic force microscope images of the respective molecules (ssDNA + SSB image is representational only; see Materials and Methods). Scale bars represent 400 nm.

Here, we employ solid-state (SS) nanopores[7, 8] to study the interactions of *E. coli* SSB (henceforth referred to simply as SSB) with DNA under high ionic strength conditions. In this approach, single molecules or molecular constructs are probed electrically as they are threaded

through a nanometer-scale aperture one at a time (Figure 1a). There have been a limited number of reports using this system to characterize DNA–protein interactions, the earliest of which demonstrated both global[9] and local[10] attachment of RecA proteins to double-stranded (ds) DNA. Subsequent studies have focused on other systems such as histone structures,[11] methylcytosine-binding proteins,[12] and streptavidin-conjugated dsDNA.[13] Recently, Japrung et al.[14] were the first to describe SSB-ssDNA measurements with SS nanopores, finding that SSB binding can be used to modulate the translocation duration and enable the detection of small molecules. However, these results also suggested strong molecule–pore interactions, which may be variable from device to device, and focused only on protein-limited conditions.

In this work, we expand the approach significantly by examining different template molecules and conditions. We first demonstrate that saturated SSB-ssDNA yields a unique electrical signature, distinct from either constituent alone. We then exploit the high selectivity of SSB for ssDNA to discriminate unlabeled dsDNA within a heterogeneous mixture. Next, we probe SSB-ssDNA binding by varying the protein concentration relative to a ssDNA template. And finally, we compare circular and linear ssDNA constructs to infer properties of the bound structure.

Results and Discussion

First, we examine translocation events associated with ssDNA and SSB separately (Figure 1b, top and middle). For each molecule, we find a narrow range of mean amplitudes (ΔG_{ssDNA} = 2.17 ± 0.54 nS; ΔG_{SSB} = 1.62 ± 0.41 nS) that cannot be separated statistically from one another. Dwell time analyses yield log-normal (i.e., Gaussian on a log scale) distributions that are similarly indistinguishable (Figure S1). For ssDNA, we note that we do not observe the consistently deep events (ΔG > 7.5 nS) described by Kowalczyk et al.[15] for the same material. While we see some large-amplitude signals, they account for only ~3% of the 551 events collected. This could be attributable to the slightly larger nanopore diameter (12 nm) used here than in the previous work (6.7–9.6 nm). This difference may significantly facilitate the passage of the ssDNA secondary structure and thus limit analyte accumulation in the sensing region of the pore. In the case of SSB alone, the observed events represent only a small portion of the total number of translocated proteins because most pass too quickly to be resolved.[16, 17] Indeed, this is supported by the exponential distribution of SSB dwell times (Figure S1), indicating that the most likely duration is below the temporal resolution of the measurement.

Next, we introduce to the same SS-nanopore device SSB and ssDNA incubated together in a molar ratio of 1:284 (ssDNA/SSB), ensuring the saturated binding of ssDNA by SSB. The resulting events are strikingly different from either molecule alone (Figure 1b, bottom), yielding a much larger mean amplitude (13.61 ± 4.30 nS) that is easily distinguished from the constituent signals despite its greater variation. The enhanced population width may be a result of molecular orientation during translocation or a subtle variation in structure from construct to construct, such as incomplete coverage. The observed increase in mean event depth agrees qualitatively with nucleoprotein filament formation because SSB-ssDNA has a large cross-sectional diameter in comparison. The formation of the complex also unravels the ssDNA (i.e., loss of complicated secondary structure in favor of wrapping around the SSB), which should produce an increase in event duration as well. While we observe such an increase (Figure S1), differentiation by this metric is challenging because of the broad, overlapping distributions of dwell time.

Because SSB has essentially no affinity for duplex DNA (cf. Figure S3), protein binding presents a potential route for high-fidelity differentiation of dsDNA from ssDNA in the SS-nanopore system. From our measurements (Figure 2a), dsDNA alone yields a narrow population of events with mean amplitude 1.81 ± 0.44 nS, similar to numerous previous reports,[18-20] a value that is not significantly different from those of either ssDNA or SSB alone (Figure 1b). However, when coincubated dsDNA, ssDNA, and SSB are introduced into the SS-nanopore, we find a bimodal distribution of event depths corresponding quantitatively to dsDNA (1.77 ± 0.20 nS) and the SSB-ssDNA complex (10.88 ± 4.45 nS).
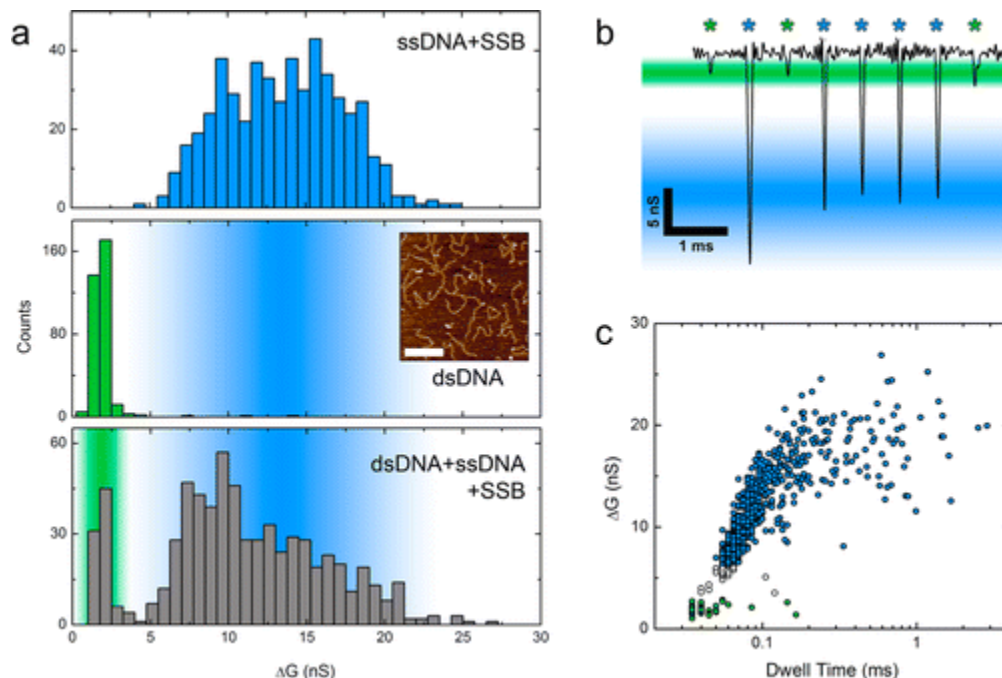

Figure 2. Differentiation of ssDNA and dsDNA using SSB. (a) Mean event amplitude histograms for ssDNA incubated with SSB (blue, same data as in Figure 1, $n = 824$), dsDNA alone (green, $n = 333$), and a mixture of dsDNA, ssDNA, and SSB (1:1:284) coincubated and measured (gray, $n = 675$). Middle inset: an atomic force microscope image of the dsDNA alone (scale bar represents 400 nm). (b) Example concatenated translocation events demonstrating the ability to differentiate dsDNA from ssDNA (bound with SSB) with single-molecule precision. Colors match those used in (a). (c) Scatter plot (dwell time vs mean event amplitude) for the coincubation of dsDNA, ssDNA, and SSB, showing the separable populations. Colors match those used in (a). Data points more than 2σ from the mean ΔG (~4.0–5.5 nS) are not identified and are unshaded (<1% of total events).

The well-separated mean event amplitude populations enable the identity of each event to be determined individually (Figure 2b) while the distinction between dsDNA and ssDNA could not be made without SSB under our conditions. Previous SS-nanopore experiments have distinguished dsDNA and ssDNA in various ways, including electrical stretching,[19] alkaline denaturation,[21] and exploiting complicated secondary structure.[15] However, these approaches considered homopolymeric ssDNA only, required chemical treatments that are incompatible with dsDNA, or relied on random (and thus variable) self-hybridization. The present approach yields

well-separated levels for heteropolymeric ssDNA in a single coincubation and is dependent only on the intrinsic nucleoprotein structure.

Figure 2c shows a scatter plot of mean ΔG and dwell time for 675 total recorded events for the mixture. The scatter in SSB-ssDNA dwell time specifically is indicative of increased interactions with the SS-nanopore walls, which is typical for protein translocations. We note that the event rate is considerably higher for SSB-ssDNA than for dsDNA despite being mixed in an equimolar ratio. Of all events for the mixture, only 83 (12%) are identifiable as dsDNA, defined as falling within 2σ of the mean dsDNA ΔG (Figure 2c). This observation is indicative of a physical difference between the two molecules under our high-ionic-strength measurement conditions. One possibility may be that the charge density of the nucleoprotein filament is significantly more negative than that of the dsDNA. Because the isoelectric point[2] of SSB is 6.0, the net charge of the construct is expected to be very negative under our conditions (pH 8.0). This may induce an electrophoretic force on SSB-ssDNA that is large compared to that on duplex DNA, allowing it to be drawn to the SS-nanopore more efficiently.
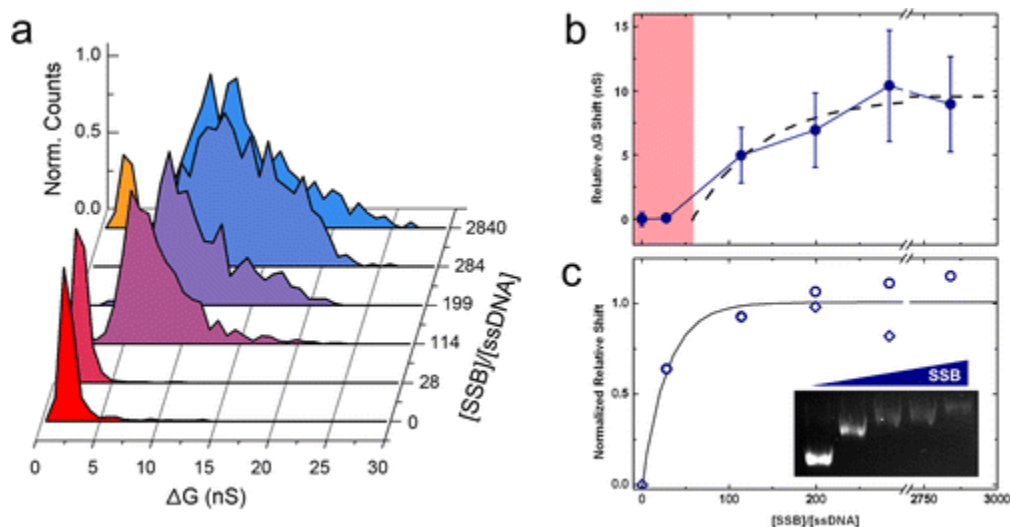

Figure 3. Titration of SSB against ssDNA. (a) Mean event amplitude histograms for ssDNA incubated with SSB in ratios of 1:0 (ssDNA alone, $n = 551$), 1:28 ($n = 989$), 1:114 ($n = 1048$), 1:199 ($n = 682$), 1:284 ($n = 517$), and 1:2840 ($n = 961$). The color shift from red to blue indicates progressive complex formation. The orange population is excess SSB (see the text). (b) Relative amplitude shift of the histograms in (a) as a function of SSB concentration. Error bars are Gaussian fit widths, and the dashed line is an asymptotic fit to the data. The shaded area indicates the apparent resolution limit. (c) Band shift analysis for two gel shift assays over the same range of relative SSB concentration. Note the strong shift even for small amounts of SSB (1:28). The solid line is an asymptotic fit to the data. The inset shows an example gel (circle data points).

To further explore SSB-ssDNA interactions, we now study a titration series. Figure 3a shows a series of mean event amplitude histograms resulting from ssDNA incubated with SSB at molar ratios ranging from 1:0 (no protein) to 1:2840 (a large excess of protein). In each measurement, a single population attributable to the nucleoprotein complex is observed, the center of which shifts as the SSB availability is increased. This is in contrast to the alternate possibility of two

discrete amplitude levels representing naked and saturated ssDNA, between which the relative occupancy shifts with SSB concentration. The explanation for these two prospective states is rooted in the binding cooperativity.[2]

In positive or "unlimited" cooperativity, the binding of one ligand to a template ssDNA will enhance its affinity for additional ligands. In that case, a given molecule is likely to be either mostly unbound or fully occupied by ligands, thus resulting in a two-level state. Unlimited cooperativity is typical of the $(SSB)_{35}$ binding mode. In limited cooperativity, an equilibrium state exists between bound tetramers and dimerized tetramers (octamers).[22] As a result, on average, each ssDNA in a mixture is bound to roughly the same number of SSBs with little or no apparent preference for molecules already occupied by proteins. This limited cooperativity has been described for the $(SSB)_{65}$ binding mode but is not thought[2] to hold for $(SSB)_{56}$. The single shifting population we see in our SS-nanopore measurements is consistent with the $(SSB)_{65}$ limited cooperativity model, as expected for the high-ionic-strength conditions we use.

The transition from ssDNA to the SSB-ssDNA complex level appears to be semisigmoidal in shape (Figure 3b), which is often associated with high cooperativity in protein binding assays.[23-25] Here, however, the trend results from the limited temporal resolution of the system. Because all measured translocation events in this report are brief (on the order of 100 μs) and the mostly naked ssDNA takes on a small profile (c.f. Figure 1b inset), features such as discrete SSBs bound to ssDNA are likely to travel through the sensing region too rapidly to be detectable. The sensing of sparse proteins is further limited by the negative net charge of the protein under our measurement conditions, resulting in an increased translocation speed for bound regions. Limited time resolution will prevent these regions from contributing to the average event amplitude. Indeed, an electromobility shift assay (Figure 3c) demonstrates that the molecular weight of ssDNA is increased even for a small amount of SSB (1:28). We expect that high-bandwidth electrical recordings[16, 26] could be more capable of resolving these sparse proteins in SS-nanopores, thus reducing the resolution limit (shaded region in Figure 3c).

For both the SS-nanopore measurements and the gel, we estimate nucleoprotein saturation at a molar ratio of about 1:114. Considering the net length of the ssDNA used in these experiments (7249 nt), this ratio yields an estimate of 64 nt per SSB, very close to the 65 nt occupied in the $(SSB)_{65}$ binding mode. We note that this does not allow for the presence of intermediate "linker" ssDNA that has been observed between SSB octamers in a nucleosome-like structure.[27, 28] We suggest that the observed complete saturation is due to a combination of high protein concentration and the known capacity of SSB to diffuse along ssDNA,[29] facilitating close packing.

Thus far, all ssDNA measurements reported in this work have been made using circular ssDNA. We now compare this circular ssDNA to a linearized form of the same molecule. Figure 4a shows a scatter plot of event duration vs mean amplitude together with accompanying histograms for the circular ssDNA after incubation with SSB at a molar ratio of 1:284 (ssDNA/SSB). As described above, we find a single, broad distribution for each attribute. The duration data yield a mean value of 82 (+29/–22) μs, with a significant tail of long-duration events due to interactions with the nanopore walls. For event amplitude, the broad distribution is again due to the orientation or structure variation of nucleoprotein filaments during translocation.

We can use the fact that ΔG scales linearly with the analyte cross-sectional area[30] to estimate the size of translocating filaments. Using the dsDNA data (Figure 2a) as a standard of known diameter (2.2 nm), the mean SSB-ssDNA amplitude of 12.6 ± 4.3 nS suggests the passage of a molecule with a diameter of 4.7–6.7 nm. As a globular tetrameric protein, SSB alone has a diameter[31] of 5.6 nm, so surprisingly, this amplitude is consistent with only the passage of one nucleoprotein filament and not two parallel filaments in a circular conformation.
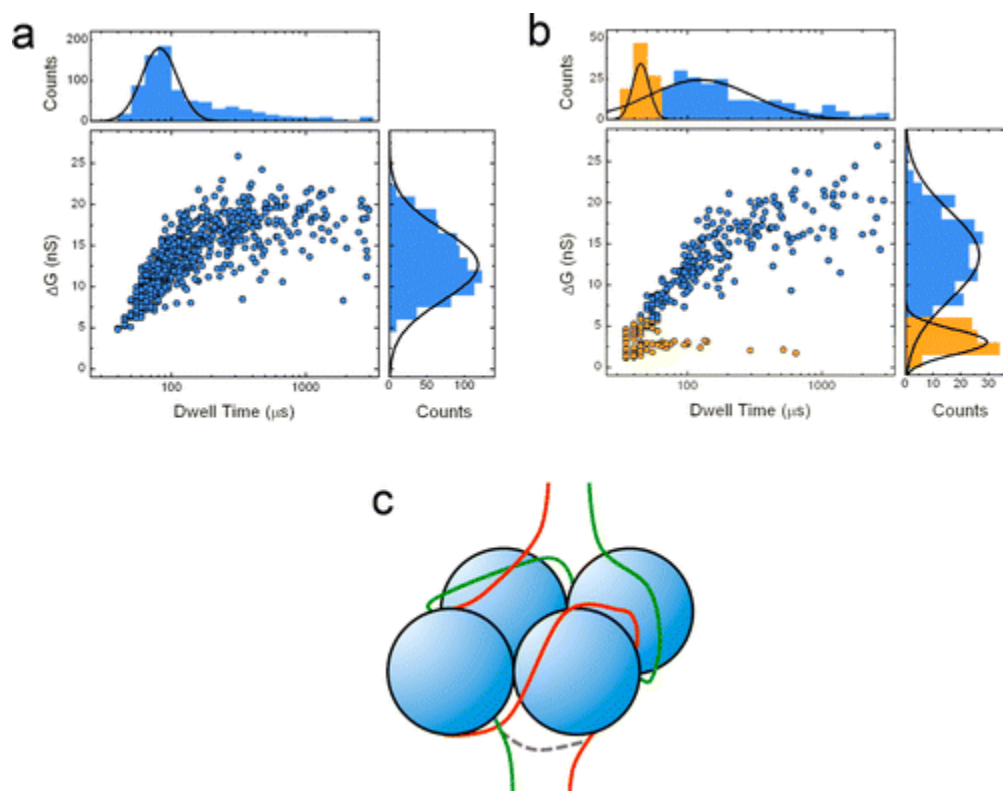

Figure 4. Comparison of circular and linearized nucleoprotein filaments. Scatter plot and accompanying duration (top) and amplitude (right) histograms for (a) circular ($n = 517$) and (b) linearized ($n = 306$) M13mp18 ssDNA incubated with SSB. Solid lines are Gaussian fits to the data. In (b), the orange population is excess SSB (see the text). (c) Proposed interpretation of the $(SSB)_{65}$ binding mode. Two regions of the same ssDNA (red and green) each interact with two binding domains of the tetrameric SSB (blue). Lagging (below) and leading (above) strands can each repeat this structure to form a nucleoprotein filament. This binding can occur with disparate regions of ssDNA or neighboring regions (gray dashed line connecting at the bottom).

Figure 4b shows an equivalent measurement repeated for SSB bound to linearized ssDNA. A population emerges with a shorter duration of 45 (+7/–6) μs and a lower amplitude of 2.5 ± 0.8 nS. We attribute these events to SSB, which is present in excess due to enzymatic and purification losses incurred during ssDNA linearization (Materials and Methods). Significantly, we still observe a major population of events with the same characteristics as for the circular SSB-ssDNA data, having a duration of 124.8 (+179/–74) μs and a mean amplitude of 13.7 ± 5.2 nS. We interpret these data to suggest that both the circular and linearized forms of the SSB-ssDNA filament have a similar structure inside the pore, consisting of ssDNA bound to a single chain of proteins. A possible conformation that could result in this structure is shown in

Figure 4c, wherein ssDNA interacts with each monomer of the SSB tetramer, but these ssDNA regions can be either contiguous or disparate. Such a conformation could explain how both circular and linearized ssDNA can "braid" around SSB, resulting in similar structures. In this way, the $(SSB)_{65}$ binding mode is maintained (consistent with the current understanding of SSB-ssDNA interactions[32]) but results in a thin filament as implied by our data. A possible alternative explanation is that our initial measurements are size-selective toward nucleoprotein filaments formed with ssDNA in solution that have been linearized due to nicking. However, we consider this unlikely because the titration of SSB beyond ssDNA saturation does not result in a strong decrease in the event rate and because the diameters of our SS-nanopore devices would not explicitly prevent the passage of constructs in a circular conformation. Additionally, we do not observe linearized ssDNA in our gel analyses of the starting material (Figures S4 and S5).

Conclusions

We have investigated the interaction of SSB with ssDNA using an SS-nanopore platform. We first demonstrated that the saturated SSB-ssDNA complex results in dramatically different electrical translocation signals than either constituent alone. This is a result of the larger macromolecular structure of the complex, which stretches the ssDNA and removes its secondary structure. Next, we used the high selectivity of SSB to show that dsDNA could be differentiated from ssDNA with great efficacy and at the single-molecule level.

We then investigated the concentration-dependent binding of SSB to ssDNA through a titration series, finding a gradual shift in mean event amplitude that corresponded to limited cooperativity among proteins. The shift in electrical signal correlated with gel elecrophoresis measurements and indicated SSB saturation at a molar ratio of about 1:114. This suggests a binding length of 64 nt, in close agreement with the known $(SSB)_{65}$ binding mode. We note that a previous study[14] was able to resolve the very sparse attachment of SSB to ssDNA. However, this was likely enabled by strong interactions with the SS-nanopore surface that do not appear to be as prevalent here.

Finally, we compared the event properties of circular and linearized ssDNA bound by SSB. We found that both samples resulted in quantitatively similar translocation characteristics, suggesting a similar nucleoprotein filament structure regardless of ssDNA conformation. Previous studies of SSB-ssDNA using transmission electron microscopy[27] and atomic force microscopy[28] have described circular nucleoprotein filaments. Our results may stem from the very high ionic strength and SSB concentration used in our experiments. These conditions were not achievable in the past approaches, where imaging required dried samples and exotic chemical treatments to improve sample quality. It is therefore possible that our results may more closely reflect the in situ structure in high-ionic-strength environments.

Materials and Methods

Biomolecule Preparation

M13mp18 ssDNA (7249 nt, 250 ng/µL), M13mp18 RF I dsDNA (7249 bp, 100 ng/µL) (New England BioLabs, Ipswich, MA), and *Escherichia coli* SSB (4470 ng/µL; Sigma-Aldrich, St.

Louis, MO) were obtained commercially and stored at −20 °C prior to use. DNA and SSB were prepared for individual measurements by adding 1 M KCl, 10 mM tris, and 1 mM EDTA (pH 8.0) to stock solutions to obtain the indicated concentrations. In coincubations, reaction mixtures were left overnight at room temperature prior to measurement.

Linear M13mp18 ssDNA was prepared by enzymatic digestion of a *Bam*HI restriction site. A 25 nt DNA oligonucleotide with complementarity to M13mp18 (sequence 5′-ACCGAGCTCGAATTCGTAATCATGG-3′; Integrated DNA Technologies, Coralville, IA) was resuspended at a concentration of 4 mg/mL in 10 mM Tris buffer plus 1 mM EDTA (pH 8) and stored at −20 °C. To prepare a hybridization reaction, circular ssDNA and the oligonucleotide were combined at final concentrations of 20 and 160 nM, respectively, held at 95 °C for 3 min, and cooled to room temperature over 30 min. Restriction digestion was performed using 10 μL of the hybridization reaction, 20 U (1 μL) of *Bam*HI restriction endonuclease (New England BioLabs, Ipswich, MA), 1.5 μL of 10× CutSmart Buffer (New England BioLabs, Ipswich, MA), and 2.5 μL of deionized water incubated at 37 °C for 1.5 h. The reaction product was loaded onto a 0.8% agarose gel, and the resulting band was excised and then purified using a Promega Wizard SV gel and PCR clean-up kit.

Solid-State Nanopore Fabrication

Silicon chips, each supporting a window of silicon nitride (24.5 nm thick as measured by ellipsometry) were obtained commercially (Norcada, Inc., Alberta, Canada). A helium ion microscope (Carl Zeiss Orion PLUS, Peabody, MA) was used to produce SS-nanopores with diameters of 11–13 nm, following a procedure described elsewhere.[33] All investigated devices exhibited a linear *I–V* curve and had a low-noise baseline current that was used to confirm the pore diameter in situ.

DNA Translocation Measurements

Solvent conditions used for the presented measurements were 1 M KCl, 10 mM tris, and 1 mM EDTA (pH 8.0). Unless otherwise noted, the final concentration of DNA introduced into the device was 2.5 ng/μL, with SSB at relative concentrations as described in the text. A patch-clamp amplifier (Axopatch 200B, Molecular Devices, Sunnyvale, CA) with a four-pole Bessel filter of 100 kHz was used both to apply a 200 mV bias across the membrane and record the ionic current. The electrical signal was sampled at 250 kHz and subjected to an additional low-pass filter of 30 kHz prior to analysis using custom LabView software.

Titration Gel Electrophoresis Assay

Twenty-five nanograms of circular ssDNA were incubated overnight in a solution of 1 M KCl, 10 mM tris, and 1 mM EDTA (pH 8.0) at room temperature with varying amounts of SSB according to the ratios noted in the text. Mixtures were loaded directly onto a 1% agarose gel prepared with a Tris/borate/EDTA buffer solution (pH 8.3) and an intercalating dye (ethidium bromide solution, Promega Biosciences, San Luis Obispo, CA).

Atomic Force Microscopy

ssDNA, dsDNA, and SSB were suspended individually at concentrations of 1 nM, 3 nM, and 1.5 μM, respectively, in 10 mM KCl and 25 mM $MgCl_2$ and deposited onto freshly cleaved mica substrates (Ted Pella, Inc., Redding, CA). After 30 s, the samples were lightly rinsed with deionized water and dried under compressed air flow through a 0.2 μm filter. The SSB-ssDNA reaction was carried out by incubating 1 nM circular ssDNA with 1.5 μM SSB in 10 mM KCl overnight at room temperature. $MgCl_2$ was added to the sample to a final concentration of 25 mM and then immediately deposited onto mica as described above. All images were captured with an MFP3D AFM (Asylum Research, Santa Barbara, CA) operated in tapping mode. We note that SSB-ssDNA incubation at high monovalent salt concentration interfered with the deposition process, so the nucleoprotein filament image is representational only.

Acknowledgment

References

1. Meyer, R. R.; Laine, P. S. The single-stranded DNA-binding protein of Escherichia coli Microbiol. Rev. **1990**, 54, 342– 80 Google Scholar

2. Lohman, T. M.; Ferrari, M. E. Escherichia coli single-stranded DNA-binding protein: multiple DNA-binding modes and cooperativities Annu. Rev. Biochem. **1994**, 63, 527– 570 Google Scholar

3. Gu, P.; Deng, W.; Lei, M.; Chang, S. Single strand DNA binding proteins 1 and 2 protect newly replicated telomeres Cell Res. **2013**, 23, 705– 719 Google Scholar

4. Huang, Y.; Chang, X.; Lee, J.; Cho, Y. G.; Zhong, X.; Park, I. S.; Liu, J. W.; Califano, J. A.; Ratovitski, E. A.; Sidransky, D.; Kim, M. S. Cigarette smoke induces promoter methylation of single-stranded DNA-binding protein 2 in human esophageal squamous cell carcinoma Int. J. Cancer **2011**, 128, 2261– 2273 Google Scholar

5. Miao, Y.; Jiang, J.; Ren, Y.; Zhao, Z. The single-stranded DNA-binding protein WHIRLY1 represses WRKY53 expression and delays leaf senescence in a developmental stage-dependent manner in Arabidopsis Plant Physiol. **2013**, 163, 746– 756 Google Scholar

6. Karan, R.; DasSarma, P.; Balcer-Kubiczek, E.; Weng, R. R.; Liao, C. C.; Goodlett, D. R.; Ng, W. V.; Dassarma, S. Bioengineering radioresistance by overproduction of RPA, a mammalian-type single-stranded DNA-binding protein, in a halophilic archaeon Appl. Microbiol. Biotechnol. **2014**, 98, 1737– 1747 Google Scholar

7. Dekker, C. Solid-state nanopores Nat. Nanotechnol. **2007**, 2, 209– 215 Google Scholar

8. Wanunu, M. Nanopores: A journey towards DNA sequencing Phys. Life Rev. **2012**, 9, 125– 158 Google Scholar

9. Smeets, R. M. M.; Kowalczyk, S. W.; Hall, A. R.; Dekker, N. H.; Dekker, C. Translocation of RecA-Coated Double-Stranded DNA through Solid-State Nanopores Nano Lett. **2009**, 9, 3089– 3095 [Google Scholar](#)

10. Kowalczyk, S. W.; Hall, A. R.; Dekker, C. Detection of Local Protein Structures along DNA Using Solid-State Nanopores Nano Lett. **2010**, 10, 324– 328 [Google Scholar](#)

11. Soni, G. V.; Dekker, C. Detection of Nucleosomal Substructures using Solid-State Nanopores Nano Lett. **2012**, 12, 3180– 3186 [Google Scholar](#)

12. Shim, J.; Humphreys, G. I.; Venkatesan, B. M.; Munz, J. M.; Zou, X.; Sathe, C.; Schulten, K.; Kosari, F.; Nardulli, A. M.; Vasmatzis, G.; Bashir, R. Detection and quantification of methylation in DNA using solid-state nanopores Sci. Rep. **2013**, 3, 1389 [Google Scholar](#)

13. Carlsen, A. T.; Zahid, O. K.; Ruzicka, J. A.; Taylor, E. W.; Hall, A. R. Selective Detection and Quantification of Modified DNA with Solid-State Nanopores Nano Lett. **2014**, 14, 5488– 5492 [Google Scholar](#)

14. Japrung, D.; Bahrami, A.; Nadzeyka, A.; Peto, L.; Bauerdick, S.; Edel, J. B.; Albrecht, T. SSB Binding to Single-Stranded DNA Probed Using Solid-State Nanopore Sensors J. Phys. Chem. B **2014**, 18, 11605– 11612 [Google Scholar](#)

15. Kowalczyk, S. W.; Tuijtel, M. W.; Donkers, S. P.; Dekker, C. Unraveling Single-Stranded DNA in a Solid-State Nanopore Nano Lett. **2010**, 10, 1414– 1420 [Google Scholar](#)

16. Larkin, J.; Henley, R. Y.; Muthukumar, M.; Rosenstein, J. K.; Wanunu, M. High-Bandwidth Protein Analysis Using Solid-State Nanopores Biophys. J. **2014**, 106, 696– 704 [Google Scholar](#)

17. Plesa, C.; Kowalczyk, S. W.; Zinsmeester, R.; Grosberg, A. Y.; Rabin, Y.; Dekker, C. Fast Translocation of Proteins through Solid State Nanopores Nano Lett. **2013**, 13, 658– 663 [Google Scholar](#)

18. Li, J. L.; Gershow, M.; Stein, D.; Brandin, E.; Golovchenko, J. A. DNA molecules and configurations in a solid-state nanopore microscope Nat. Mater. **2003**, 2, 611– 615 [Google Scholar](#)

19. Skinner, G. M.; van den Hout, M.; Broekmans, O.; Dekker, C.; Dekker, N. H. Distinguishing Single- and Double-Stranded Nucleic Acid Molecules Using Solid-State Nanopores Nano Lett. **2009**, 9, 2953– 2960 [Google Scholar](#)

20. Storm, A. J.; Chen, J. H.; Zandbergen, H. W.; Dekker, C. Translocation of double-strand DNA through a silicon oxide nanopore Phys. Rev. E **2005**, 71, 051903 [Google Scholar](#)

21. Fologea, D.; Gershow, M.; Ledden, B.; McNabb, D. S.; Golovchenko, J. A.; Li, J. L. Detecting single stranded DNA with a solid state nanopore Nano Lett. **2005**, 5, 1905– 1909 [Google Scholar](#)

22. Raghunathan, S.; Kozlov, A. G.; Lohman, T. M.; Waksman, G. Structure of the DNA binding domain of E. coli SSB bound to ssDNA Nat. Struct. Biol. **2000**, 7, 648– 652 [Google Scholar](#)

23. Ferrari, M. E.; Bujalowski, W.; Lohman, T. M. Cooperative binding of Escheria coli SSB tetramers to single-stranded DNA in the (SSB)35 binding mode J. Mol. Biol. **1994**, 236, 106– 123 Google Scholar

24. Menetski, J. P.; Kowalczykowski, S. C. Interaction of RecA protein with single-stranded DNA: Quantitative aspects of binding affinity modulation by nucleotide cofactors J. Mol. Biol. **1985**, 181, 281– 295 Google Scholar

25. Wienken, C. J.; Baaske, P.; Rothbauer, U.; Braun, D.; Duhr, S. Protein-binding assays in biological liquids using microscale thermophoresis Nat. Commun. **2010**, 1, 100 Google Scholar

26. Rosenstein, J. K.; Wanunu, M.; Merchant, C. A.; Drndic, M.; Shepard, K. L. Integrated nanopore sensing platform with sub-microsecond temporal resolution Nat. Methods **2012**, 9, 487– U112 Google Scholar

27. Chrysogelos, S.; Griffith, J. Escheria coli single-strand binding protein organizes single-stranded DNA in nucleosome-like units Proc. Natl. Acad. Sci. U.S.A. **1982**, 79, 5803– 5807 Google Scholar

28. Hamon, L.; Pastre, D.; Dupaigne, P.; Le Breton, C.; Le Cam, E.; Pietrement, O. High-resolution AFM imaging of single-stranded DNA-binding (SSB) protein-DNA complexes Nucleic Acids Res. **2007**, 35, e58 Google Scholar

29. Roy, R.; Kozlov, A. G.; Lohman, T. M.; Ha, T. SSB protein diffusion on single-stranded DNA stimulates RecA filament formation Nature **2009**, 461, 1092– 1097 Google Scholar

30. Hall, A. R.; Keegstra, J. M.; Duch, M. C.; Hersam, M. C.; Dekker, C. Measuring single-wall carbon nanotubes with solid-state nanopores Methods Mol. Biol. **2012**, 870, 227– 239 Google Scholar

31. Erickson, H. P. Size and Shape of Protein Molecules at the Nanometer Level Determined by Sedimentation, Gel Filtration, and Electron Microscopy Biol. Proced. Online **2009**, 11, 32– 51 Google Scholar

32. Raghunathan, S.; Kozlov, A. G.; Lohman, T. M.; Waksman, G. Structure of the DNA binding domain of E-coli SSB bound to ssDNA Nat. Struct. Biol. **2000**, 7, 648– 652 Google Scholar

33. Yang, J.; Ferranti, D. C.; Stern, L. A.; Sanford, C. A.; Huang, J.; Ren, Z.; Qin, L.-C.; Hall, A. R. Rapid and precise scanning helium ion microscope milling of solid-state nanopores for biomolecule detection Nanotechnology **2011**, 22, 285310 Google Scholar

Supplementary Information: Nanopore Analysis of Single-Stranded Binding Protein Interactions with DNA

Michael M. Marshall[1], Jan Ruzicka[1], Osama K. Zahid[2], Vincent C. Henrich[3], Ethan W. Taylor[1], and Adam R. Hall[2,4#]
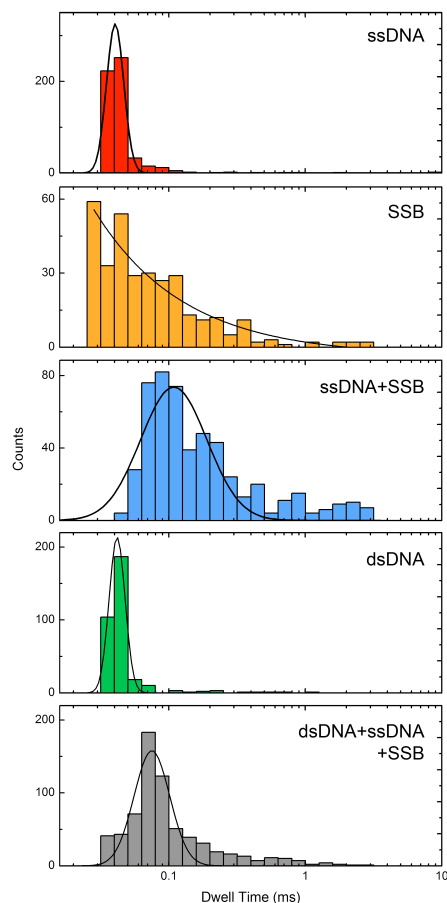
Figure S1. Dwell time analyses Event duration histograms for indicated constituents and mixtures. Colors and event counts (*n*) match those found in Figs. 1a and 2b from the main text. Each histogram is fit by a single Gaussian (solid line) except for the SSB (orange), which is fit by a single exponential. The large duration tails on the ssDNA/SSB mixture (blue) and the dsDNA/ssDNA/SSB mixture (grey) are a result of strong interactions between the SSB-ssDNA complex and the nanopore walls. Discrepancy from the fit for low dwell times in the dsDNA+ssDNA+SSB plot are due to bare dsDNA.
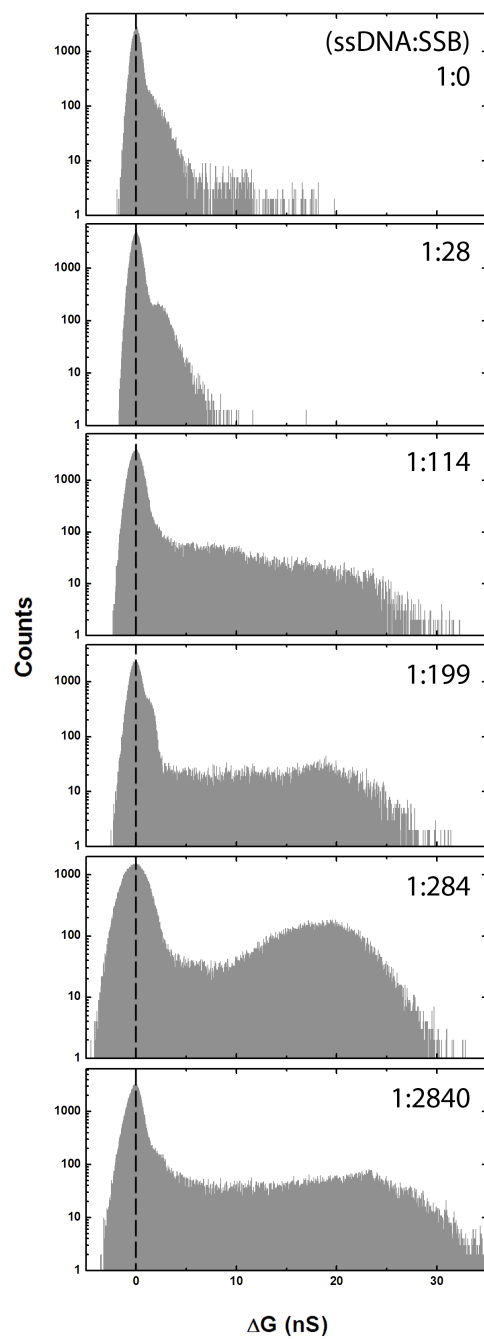
Figure S2. All-points histograms All-points histograms for SSB titration measurements. Dashed line indicates the baseline conductance points.
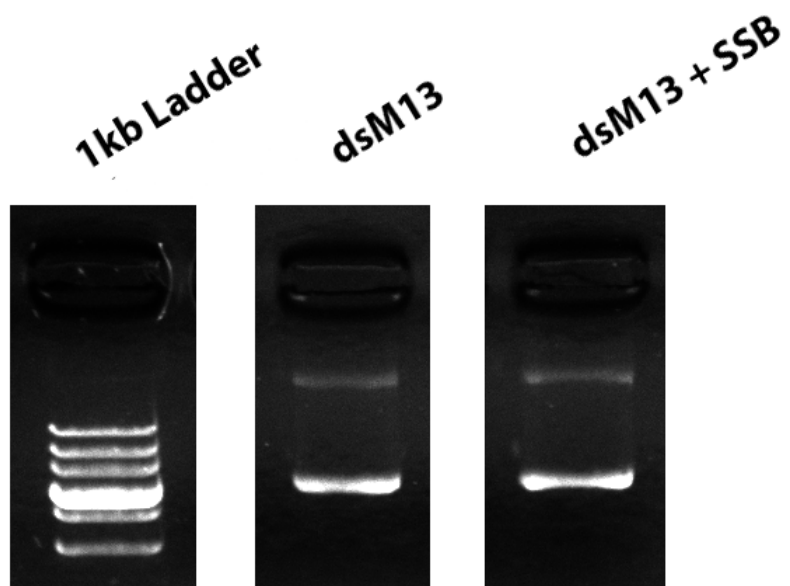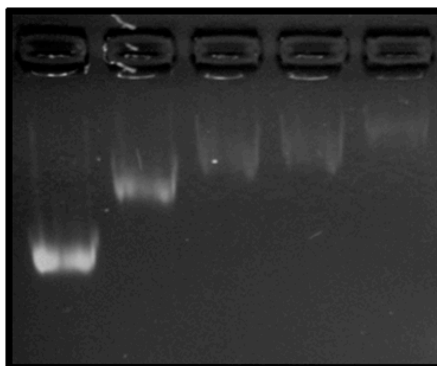
Figure S3. Gel analysis of dsDNA-SSB interaction Agarose gel electrophoresis of M13mp18 dsDNA alone (left) and incubated with SSB (1:284, right). The minor lagging band indicates nicked dsDNA plasmid. No interaction with SSB is observed.
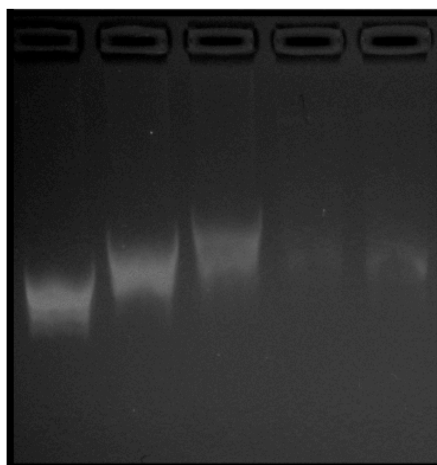
Figure S4. SSB-ssDNA electromobility shift assays Two SSB-ssDNA gel shift assay. The top gel is the same one shown in the main text. In both images, as SSB ratio increases bands dim due to loss of secondary structure with which intercalating dye can interact.
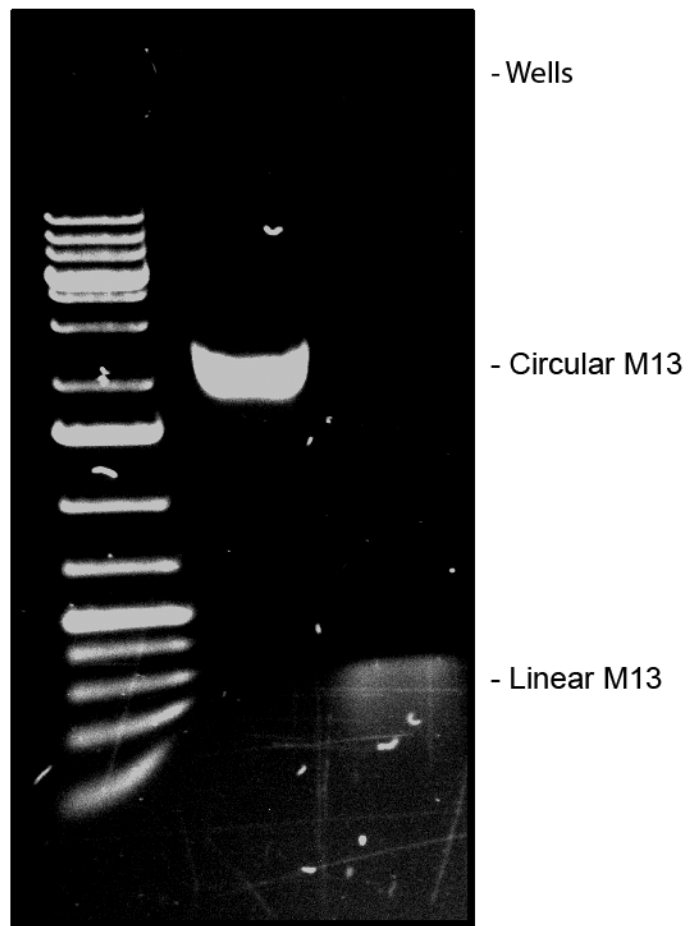
Figure S5. Linearization of circular M13mp18 ssDNA Gel electrophoresis showing a 1 kb dsDNA ladder (lane 1), M13mp18 ssDNA in its native circular form (lane 2) and linearized using the protocol in the main text (lane 3).